Published in final edited form as:
Physiol Behav. 2007 October 22; 92(3): 507–519. doi:10.1016/j.physbeh.2007.04.028.

CANNABINOID-INDUCED HYPERPHAGIA: CORRELATION WITH INHIBITION OF PROOPIOMELANOCORTIN NEURONS?

Jennie Ho, **Jeremy M. Cox**, and **Edward J. Wagner**
Department of Basic Medical Sciences, Western University of Health Sciences, Pomona, CA 91766

Abstract

We tested the hypothesis that cannabinoids modulate feeding in male guinea pigs, and correlated cannabinoid-induced changes in feeding behavior with alterations in glutamatergic synaptic currents impinging upon proopiomelanocortin (POMC) neurons of the hypothalamic arcuate nucleus. Feeding experiments were performed as follows: after a three-day acclimation period, animals were weighed and injected with either the CB1 receptor agonist WIN 55,212-2 (1 mg/kg, s.c.), antagonist AM251 (3 mg/kg, s.c.) or their cremophore/ethanol/saline vehicle (1:1:18; 1 ml/kg, s.c.) each day for seven days. WIN 55,212-2 increased, whereas AM251 decreased, the rate of cumulative food intake. The agonist effect was manifest primarily by increases in meal frequency and the amount of food eaten per meal. By contrast, the antagonist effect was associated with decreases in meal frequency, duration and weight loss. For the electrophysiological experiments, we performed whole-cell patch clamp recordings from POMC neurons in hypothalamic slices. WIN 55,212-2 decreased the amplitude of evoked, glutamatergic excitatory postsynaptic currents (eEPSCs) and increased the S2:S1 ratio. Conversely, AM251 increased eEPSC amplitude *per se*, and blocked the inhibitory effects of the agonist. WIN 55,212-2 also decreased miniature EPSC (mEPSC) frequency; whereas AM251 increased mEPSC frequency *per se*, and again blocked the inhibitory effect of the agonist. A subpopulation of cells exhibited an agonist-induced outward current, which was blocked by AM251, associated with increased conductance and reversed polarity near the Nernst equilibrium potential for K^+. These data demonstrate that cannabinoids regulate appetite in the guinea pig in part through both presynaptic and postsynaptic actions on anorexigenic POMC neurons.

Keywords

feeding; glutamate; potassium conductance; CB1 receptor; POMC; arcuate; electrophysiology

Introduction

There is a growing appreciation of the role cannabinoids play in regulating homeostatic behaviors governed by the hypothalamus including, but not limited to, reproduction and feeding. For example, cannabinoids increase appetite in humans and various rodent animal models [1–5], and it is thought that the hyperphagia induced by cannabinomimetics can be of clinical utility in combating the body wasting observed with cancer chemotherapy and AIDS [2,6,7]. On the other hand, cannabinoid CB1 receptor antagonists are being used as a

Author to whom correspondence should be addressed: Edward J. Wagner, Ph.D., Department of Basic Medical Sciences, College of Osteopathic Medicine, Western University of Health Sciences, 309 E. Second Street, Pomona, CA 91766.

pharmacological intervention in the treatment of obesity [4,8,9] and the metabolic syndrome [10].

CB1 receptors are located in the myenteric plexus of the enteric nervous system [11], where they play an important role in regulating gastric emptying and intestinal motility [12]. CB1 receptors also are expressed in vagal afferents emanating from the gastrointestinal (GI) tract [13], and activation of these receptors inhibits glutamatergic synaptic currents in the dorsal motor nucleus of the vagus [14]. While it is clear that cannabinoids can influence appetite at the level of both the GI tract and brainstem, there is also considerable evidence to suggest that cannabinoids stimulate feeding by also acting within the hypothalamus. The hypothalamic feeding circuitry comprises orexigenic components with orexin- and melanin-concentrating hormone-containing somata in the lateral hypothalamic area [15–18], and neuropeptide Y (NPY)- and ghrelin-containing neurons in the arcuate nucleus [19–23]. The neuroanatomical substrates of the anorexigenic component include the ventromedial nucleus [24], proopiomelanocortin (POMC) neurons in the arcuate nucleus [25,26], cocaine-amphetamine-regulated transcript (CART) neurons in the arcuate, dorsomedial, lateral hypothalamic and paraventricular nuclei [27], and corticotropin-releasing hormone (CRH) neurons in the paraventricular nucleus [28]. This latter population appears to be a point of convergence for both orexigenic and anorexigenic inputs that integrates incoming information into an efferent response [18,22,28–30]. CB1 receptors are expressed in several nuclei of the hypothalamic feeding circuitry, where they are found on nerve terminals impinging upon MCH, CRH and POMC neurons [31]. In addition, hypothalamic levels of endogenous cannabinoids such as 2-arachidonyl glycerol (2-AG) are decreased by the adipostat leptin [32], which also depolarizes and increases the firing rate of POMC neurons [25,33]. Furthermore, food intake is decreased in CB1 receptor knockout mice [27,32], whereas transgenic mice deficient in the byproduct of posttranslational POMC processing, β-endorphin, exhibit rampant hyperphagia [34]. Thus, when considering the possible substrates upon which cannabinoids act to increase appetite, one must also include POMC neurons of the hypothalamic arcuate nucleus.

The purpose of the present study was test the hypothesis that cannabinoids stimulate feeding behavior in part by decreasing the excitability of POMC neurons. To this end, we employed a guinea pig animal model used in a number of different feeding, gastroenterological and metabolic studies [35–37]. We undertook a multidisciplinary approach to evaluate cannabinoid-induced changes in feeding behavior, as well as alterations in both glutamatergic synaptic input and postsynaptic K^+ conductances occurring within POMC neurons. We utilized several indices of feeding behavior, including the rate of food intake, meal frequency and duration, and the amount of food eaten per meal. Intracellular patch-clamp recordings from hypothalamic arcuate neurons were performed using an *in vitro* hypothalamic slice preparation with biocytin-filled electrodes that enabled subsequent phenotypic identification of the cells. The results reveal that the CB1 receptor agonist (R)-(+)-[2,3-dihydro-5-methyl-3-(4-morpholinylmethyl)pyrrolo[1,2,3-de]-1,4-benzoxazin-6-yl]-1-naphthalenylmethanone mesylate (WIN 55,212-2) and antagonist N-(piperidin-1-yl)-5-(4-iodophenyl)-4-methyl-1H-pyrazole-3-carboxamide (AM251) increase and decrease feeding respectively. These behavioral changes correlate in a compelling fashion with changes in glutamatergic neurotransmission and postsynaptic K^+ conductances in POMC neurons, suggesting that these neurons are indeed a critical cellular link to the orexigenic response elicited by cannabinoids.

Materials and Methods

Animals and Treatments

All animal procedures described in this study are in accordance with institutional guidelines based on NIH standards. Male Topeka guinea pigs (250–410 g) were obtained from Elm Hill

Breeding Labs (Chelmsford, MA, USA), kept under controlled temperature (69–73°F) and light (12 h on: 12 h off), and provided with food and water *ad libitum*.

Drugs

Unless otherwise specified, all drugs were purchased from Tocris Cookson, Inc. (Ellisville, MO, USA.) For the behavioral experiments, both WIN 55,212-2 and AM251 were dissolved in a mixture of cremephor/ethanol/0.9% saline (1:1:18; v/v/v). For the electrophysiology experiments, tetrodotoxin (TTX) with citrate (Alomone Labs, Jerusalem, Israel) was dissolved in UltraPure H_2O to a stock concentration of 1 mM. Arachidonyl-2′-chloroethylamide (ACEA) was dissolved in ethanol to a stock concentration of 1 mM. *cis*-4-[Phosphomethyl]-2-piperidinecarboxylic acid (CGS 19755; 10 mM) was dissolved in 0.1N NaOH and then diluted to the final volume with UltraPure H_20. WIN-55,212-2, AM251 and 2,3-dioxo-6-nitro-1,2,3,4-tetrahydrobenzo[f]quinoxaline-7-sulfonamide (NBQX) were dissolved in dimethyl sulfoxide to stock concentrations of 10 mM. Stock solutions of 6-imino-3-(4-methoxyphenyl)-1(6H)-pyridazinebutanoic acid hydrobromide (SR 95531; 10 mM) and tertiapin (1 μM; Alomone Labs) were prepared with UltraPure H_2O. Baclofen (40 mM) was dissolved in 0.1 N HCl.

Feeding behavior paradigm

The behavioral experiments were conducted using a four-cage, Comprehensive Lab Animal Monitoring System (Columbus Instruments, Columbus, OH, USA) from which we monitored four parameters of feeding: food intake, meal frequency, meal duration and the amount of food eaten per meal. An electronic balance measured the amount of food (certified guinea pig diet 5026, powdered formulation; Newco Distributors, Inc., Rancho Cucamonga, CA, USA), contained within the food dish and separate spillage container that sit atop it, with the difference being the actual amount of food consumed. Two photoelectric sensors are arrayed above the food dish, which detect each time the animal moves in for a meal. The signals generated are transmitted to an A/D converter, and digitally stored on computer. Food intake is defined as the amount of food consumed (in g) normalized to the total amount eaten over the designated six-hour observation period ranging from 08:30 – 14:30. Meal frequency equals the number of meals consumed per unit time, with a meal defined as the amount of food (in g) consumed in one sitting. Meal duration refers to the amount of time necessary to eat a meal consisting of at least 10 mg of food. The amount of food eaten per meal is defined as the amount of food eaten in a given hour relative to the total amount consumed over the six-hour evaluation period divided by the number of meals in that same hour. The animals were allowed to acclimate in the feeding chambers for six hours per day over a three-day period. Each morning they were weighed, handled, placed in their respective chambers for six hours, and then returned to their home cages. After the three-day acclimation session, we initiated the seven-day monitoring phase during which the animals were weighed, injected each morning with either WIN 55,212-2 (1 mg/kg; s.c.), AM251 (3 mg/kg; s.c.) or its cremephor/ethanol/0.9% saline vehicle (1 ml/kg; s.c.), immediately placed in their feeding chambers and then subject to continuous monitoring of each of the four above-described feeding parameters over the six-hour time span.

Tissue preparation

On the day of experimentation the animal was decapitated, its brain removed from the skull and the hypothalamus dissected. We then mounted the resultant hypothalamic block on a cutting platform that was then secured in a vibratome well filled with ice-cold, oxygenated (95% O_2, 5% CO_2) artificial cerebrospinal fluid (aCSF, in mM: NaCl, 124; $NaHCO_3$ 26; dextrose, 10; HEPES, 10; KCl, 5; NaH_2PO_4, 2.6; $MgSO_4$, 2; $CaCl_2$, 1). Five coronal slices (350 μm) through the arcuate nucleus were then cut. The slices were transferred to an auxiliary chamber containing oxygenated aCSF, and kept there until electrophysiological recording.

Electrophysiology

Whole-cell patch recordings in hypothalamic slices were performed as previously described [38]. Briefly, during the recording session, slices were maintained in a chamber perfused with a warmed (35°C), oxygenated aCSF that was identical to that described above, the exception being an increase in the $CaCl_2$ concentration to 2 mM. Artificial CSF and all drugs (diluted with aCSF) were perfused via a peristaltic pump at a rate of 1.5 ml/min. Patch electrodes were assembled from borosilicate glass (World Precision Instruments; Sarasota, FL, USA; 1.5 mm O.D.) pulled on a P-97 Flaming Brown puller (Sutter Instrument Co., Novato, CA, USA), and filled with the following (in mM): potassium gluconate, 128; NaCl, 10; $MgCl_2$, 1; EGTA, 11; HEPES, 10; ATP, 1.2; GTP, 0.4; 0.35 – 0.4% biocytin; adjusted to a pH of 7.3 – 7.4 with 1.0 N KOH; 297 – 321 mOsm. Electrode resistances varied from 3 – 8 M Ω A Multiclamp 700A preamplifier (Axon Instruments, Foster City, CA, USA) amplified potentials and passed current through the electrode. The patch electrode was advanced into the arcuate nucleus with a positive pressure applied to the back of the electrode using a 5-ml syringe connected by polyethylene tubing to the electrode holder. Once the electrode came up against a cell membrane, as indicated by a small decrease in the monitored current deflection (20–50% of the initial amplitude), a slight negative pressure was then applied via suction to form a stable gigaohm seal. We obtained whole cell recordings by applying additional suction to rupture the membrane under the electrode. Membrane currents were recorded in voltage clamp and underwent analog-digital conversion via a Digidata 1322A interface coupled to pClamp 8.2 software (Axon Instruments). The access resistance, as well as the resting membrane potential (RMP) and the input resistance (R_{in}), were monitored throughout the course of the recording. If the access resistance deviated greater than 10% of its original value, the recording was ended. Low-pass filtering of the currents was conducted at a frequency of two KHz. The liquid junction potential was calculated to be −10 mV, and is corrected for during data analysis using pClamp software.

In the studies designed to evaluate eEPSCs in arcuate neurons, concentric bipolar tungsten stimulating electrodes (World Precision Instruments) were placed 0.5 – 1.0 mm lateral to the recording electrode to deliver square-wave pulses 500 μsec in duration (0.1 Hz; 3–18 V) generated by a model S88K stimulator (Astro-Med, Inc., West Warwick, RI, USA) and converted to constant voltage by a model SIU5 stimulus isolation unit (Astro-Med). We recorded eEPSCs from a holding potential of −75 mV in the presence of SR 95531 (10 μM) to block γ-aminobutyric acid $(GABA)_A$ receptor-mediated synaptic currents. Peak eEPSC amplitudes were measured by averaging those obtained from 20 consecutive stimulations. Rare failures of the stimulus to evoke PSCs were excluded from the analyses. The time-to-peak reflects the time necessary for the inward current to descend to its maximum amplitude. The rate of eEPSC decay was calculated as the time necessary for the current to decline to one-third of its peak value. Cells were perfused with WIN 55,212-2 (1 - 3 μM) for four min and the stimulation paradigm is repeated in the presence of the agonist. To help confirm a presynaptic site of cannabinoid action, we employed the paired-pulse paradigm in which we presented successive stimuli that were separated by 75 msec from one another. CB1 receptor specificity was ascertained by evaluating CB1 receptor activation in slices pretreated with AM 251 (1 μM). We verified that the eEPSCs were ionotropic glutamate receptor-mediated by repeating the stimulation in the presence of CGS 19755 (10 μM) and NBQX (3 μM).

We recorded mEPSCs in the presence of both SR 95531 (10 μM) and TTX (500 nM) from a holding potential of −75 mV. After collecting a 3–4 min segment of baseline data, we perfused either WIN 55,212-2 (100 nM – 10 μM) or ACEA (1 μM) for four min, and then recorded mEPSCs in the presence of agonist. The threshold for mEPSC detection was set at least three pA below the baseline holding current as assessed from the headstage output, and continuously monitored throughout each 3–4 min recording period. Information on interval and amplitude

was obtained from at least 100 contiguous mEPSCs, which we used to evaluate cannabinoid-induced alterations in mEPSC frequency and amplitude as assessed from cumulative probability plots. CB1 receptor specificity was again ascertained by evaluating CB1 receptor activation in slices pretreated with AM 251 (1 μM), and the mEPSCs were pharmacologically identified using CGS 19755 (10 μM) and NBQX (3 μM).

To characterize the CB1 receptor-mediated activation of GIRK, either WIN 55,212-2 or ACEA were perfused until a new steady-state holding current was established (3–5 min). Current-voltage relationships were generated before and immediately following agonist application over a range centering on the equilibrium potential for K^+. This is accomplished with step command potentials ranging from −50 to −130 mV (1 sec duration; 10 mV increments). Blockade of the agonist-induced outward current by AM 251 served as the indication that the effect was CB1 receptor-mediated. For comparison, the ability of the $GABA_B$ receptor agonist baclofen (100 μM) to elicit its characteristic outward current was ascertained prior to, and in the presence of, the GIRK channel blocker tertiapin (10 nM).

Immunohistofluorescence

After recording, some slices were processed for phenotypic identification as described previously [39]. Briefly, slices were fixed with either 4% paraformaldehyde (PFM) in Sorensen's phosphate buffer (pH 7.4) for 90–180 min. They then were immersed overnight in 20% sucrose dissolved in Sorensen's buffer, and frozen in Tissue-Tek embedding medium (Miles, Inc., Elkhart, IN, USA) the next day. Coronal sections (20 μm) were cut on a cryostat and mounted on charged slides. These sections were washed with 0.1 M sodium phosphate buffer (pH 7.4). All sections were then processed with streptavidin-cy2 (Amersham Biosciences, Piscataway, NJ, USA) at a 1:300 dilution. After localizing the biocytin-filled neuron, the slides containing the appropriate sections were reacted with either a β-endorphin antiserum [40] or an antibody directed against α-melanocyte-stimulating hormone (α-MSH; Immunostar, Inc., Hudson, WI, USA) at a 1:1000 or 1:200 dilution, respectively, using fluorescence immunohistochemistry [39].

Statistics

Variance homogeneity was evaluated using Levene's test. Comparisons between groups were performed using either the Student's t-test or the Mann-Whitney U-test. Comparisons between more than two groups were accomplished via the analysis of variance (ANOVA) followed by either the Least Significant Difference (LSD) test or median-notched box-and-whisker analysis, or the Kruskal-Wallis test followed by either the Mann-Whitney U-test or median-notched box-and-whisker analysis. Differences were considered statistically significant if the probability of error was less than 5%.

Results

Figure 1 depicts food intake as a function of time on four representative days (days 2–5) over the course of the seven-day monitoring period. Multifactorial ANOVA revealed that, compared to vehicle-treated controls, systemic administration of either the CB1 receptor agonist WIN 55,212-2 (1 mg/kg; s.c.) or antagonist AM251 (3 mg/kg; s.c.) resulted in a significant main effect (day 2: F-ratio = 81.07, $p<0.0001$; day 3: F-ratio = 49.54, $p<0.0001$; day 4: F-ratio = 61.43; $p<0.0001$; day 5: F-ratio = 152.2; $p<0.0001$) on the rate of food consumption. WIN 55,212-2 increased the rate of food intake, whereas AM251 decreased it. These effects became apparent 1–2 hour following their administration just prior to beginning the evaluation period, and lasted up to 4–6 hours into the monitoring. The agonist-induced increase in the cumulative rate of food intake shown for day 5 (like all other days) was completely abolished by co-administration of antagonist. There was no change in the total amount of food eaten over the

course of the six-hour evaluation period (not shown). We also examined cannabinoid effects on meal frequency, meal duration and the amount of food eaten per meal. Figure 2 shows the effect of WIN 55,212-2 and AM251 on meal frequency ascertained every hour during the evaluation period. Multifactorial ANOVA again revealed significant main drug effect (F-ratio = 13.41, $p<0.0001$), as well as a significant interaction (F-ratio = 4.77, $p<0.0001$). WIN 55,212-2 increased meal frequency during the second hour, followed by a pronounced decrease during hours 3–6. AM251 completely blocked the agonist-induced increase meal frequency, and attenuated the prolonged decrease in meal frequency observed during the mid- to latter stages of the monitoring period. On the other hand, AM251 produced a decrease in meal frequency during hour 1, which was reversed by co-administration of the agonist. The increase in the rate of food consumption and meal frequency produced by WIN 55,212-2 was associated with a modest increase in meal duration (Figure 3) during hour 1 and a dramatic increase in the amount of food eaten per meal (Figure 4). These effects were eliminated by co-administration of the antagonist. WIN 55,212-2 was without effect on the rate of weight gain (Figure 5). Conversely, AM251 markedly decreased meal duration (Figure 3) and elicited a significant reduction in weight gain (Figure 5), and these effects were at least partially reversed by co-administration of the agonist. AM251 did not affect the amount of food eaten per meal, *per se* (Figure 4). Collectively, this indicates that CB1 receptor activation by both exogenous and endogenous cannabinoid agonists increases feeding behavior, whereas CB1 receptor antagonism suppresses it.

We then wanted to determine if the increased appetite produced by activation of CB1 receptors was associated with a decrease in glutamatergic synaptic input onto anorexigenic POMC neurons. Accordingly, we performed whole-cell patch-clamp recordings from arcuate neurons in hypothalamic slices. Figure 6 shows traces of excitatory postsynaptic currents (EPSCs) evoked by square-wave pulses delivered by a bipolar tungsten stimulating electrodes positioned 0.5–1.0 μm lateral to the recording electrode. Bath application of WIN 55,212-2 (1 μM) reduced the amplitude of evoked EPSCs (eEPSCs) that were subsequently abolished in the presence of the ionotropic glutamate receptor antagonists NBQX (3 μM) and CGS 19755 (10 μM; Figures 6A and 6C). On the other hand, AM251 (1 μM) *per se* increased eEPSC amplitude, and when co-administered with WIN 55,212-2 it blocked the inhibitory effect of the agonist (Figures 6B and 6C). Neither WIN 55,212-2 nor AM251 had any effect on the rate of rise or the decay of the eEPSCs (not shown). Further analysis using the paired-pulse paradigm revealed that the agonist-induced reduction in eEPSC amplitude was associated with an increase in the S2:S1 ratio (Figures 6D–6F). To verify that the agonist-induced reduction could be attributed to a presynaptic mechanism of action, we next performed an analysis of miniature EPSCs (mEPSCs) recorded in the presence of 500 nM TTX. Figures 7 and 8 show representative traces of mEPSCs recorded from arcuate neurons. Varying doses of WIN 55,212-2 (100 nM & 10 μM) produced graded increases in the interval between contiguous mEPSCs, which effectively translates into a decrease in mEPSC frequency, with no discernable effect on mEPSC amplitude (Figure 7A). These observations are substantiated further by the cumulative probability plots shown in Figure 7B. WIN 55,212-2 (100 nM) similarly, yet slightly less effectively, reduced the frequency of miniature, inhibitory postsynaptic currents (mIPSCs) recorded in the presence of TTX, NBQX and CGS 19755 from a holding potential of −30 mV (mIPSCs: 68.3 ± 7.6% of control (n = 3) vs. mEPSCs: 52.6 ± 6.5% of control (n = 5)). In addition, the selective effect of WIN 55,212-2 on mEPSC frequency was mimicked by the anandamide analog ACEA (not shown). On the other hand, AM251 both increased mEPSC frequency *per se* and blocked the diminution caused by WIN 55,212-2 (Figure 8A). The composite effects of WIN 55,212-2 and AM251 on mEPSC frequency and amplitude are summarized in Figure 8B. These data suggest that CB1 receptor activation by both exogenous and endogenous cannabinoid agonists presynaptically inhibits glutamatergic synaptic input onto arcuate neurons.

We noticed during the mEPSC experiments that approximately one-third of arcuate neurons (10/31) responded to both WIN 55,212-2 and ACEA with a change in the holding current, and thus explored this observation in greater detail. Figures 9A1 and 9B1 show representative examples of the outward current elicited by bath application of 1 μM ACEA. Current-voltage relationships generated prior to, and in the presence of, the agonist reveal that the current reverses polarity very near the Nernst equilibrium potential for K^+, and exhibits an increase in slope conductance that grows more pronounced as the membrane potential is hyperpolarized below the reversal potential (Figure 9A2). This agonist-induced outward current was blocked by AM251 (Figure 9B2), and was found to be both qualitatively (Figure 9C) and quantitatively (Figure 9D) very similar to the G-protein-gated, inwardly-rectifying K^+ current (GIRK) elicited by activation of metabotropic $GABA_B$ receptors. The activation of this postsynaptic K^+ current, as well as the presynaptic inhibition of glutamatergic synaptic input described above, was observed in POMC neurons (n = 6) subsequently identified through immunohistofluorescent visualization (Figure 10). Taken together, these data demonstrate that cannabinoids increase feeding behavior, which is associated with a presynaptic inhibition of glutamatergic neurotransmission and a postsynaptic activation of an inwardly-rectifying K^+ current within POMC neurons. This indicates that the cannabinoid modulation of appetite is mediated, at least in part, through interactions with the hypothalamic feeding circuitry.

Discussion

The results of the present study demonstrate unequivocally that cannabinoids stimulate appetite, which correlates with a decrease in the excitability of POMC neurons. These conclusions are based on the following observations: 1) CB1 receptor activation and blockade respectively increases and decreases feeding behavior as determined using four different indices: the rate of food intake, meal frequency, meal duration, the amount of food eaten per meal and change in body weight, 2) CB1 receptor activation and blockade respectively decreases and increases glutamatergic neurotransmission via a presynaptic site of action, 3) cannabinoids affect a CB1 receptor-mediated activation of an inwardly rectifying K^+ current and 4) the latter two cellular effects of cannabinoids occur in arcuate neurons subsequently identified as POMC neurons via immunohistofluorescence. The current findings also suggest that glutamatergic synaptic input onto POMC neurons is tonically inhibited by endogenous cannabinoids, which provides further evidence that these neurons are a critical target in the cannabinoid modulation of appetite.

While WIN 55,212-2 has affinity for both CB1 and CB2 receptor subtypes [41], and CB2 receptors are found in the brainstem [42], the fact that the CB1 receptor antagonist AM251 largely abolished the agonist-induced hyperphagia, decrease in eEPSC amplitude, mEPSC frequency and the activation of the inwardly-rectifying K^+ conductance clearly indicates that the effects observed in the present study are CB1 receptor-mediated. In the present study, CB1 receptor activation upon the exogenous administration of WIN 55,212-2 increased the rate of food intake, meal frequency, meal duration and the amount of food eaten per meal. Thus, exogenously administered cannabinoids increased eating efficiency. On the other hand, CB1 receptor antagonism decreased the rate of food intake, meal frequency and meal duration, indicating that endogenous cannabinoids drive appetite and food seeking behavior. The cannabinoid-induced hyperphagia that we observed in our guinea pig animal model is consistent with that reported in humans and other rodent models. Despite a limited number of controlled scientific studies, the ability of cannabinoids, in particular Δ^9-tetrahydrocannabinol (Δ^9-THC), to cause the sensation of hunger and increase food intake in humans has been recognized for centuries [2–5]. In rats and mice, exogenously administered cannabinoid agonists stimulate appetite under *ad libitum* and food-deprived conditions [1,2,43], whereas CB1 receptor antagonists suppress it [8,9]. In addition, Δ^9-THC promotes feeding in rats when focally injected into the ventromedial or lateral hypothalamus [2,4], and the satiety hormone

leptin decreases hypothalamic levels of endogenous 2-AG [32]. Moreover, both ob/ob mice (which do not produce leptin) and fa/fa rats (which do not express leptin receptors) exhibit rampant hyperphagia and weight gain [32,44,45], as well as elevated hypothalamic levels of endogenous cannabinoids [32], with respect to their wildtype counterparts. Thus, the cannabinoid regulation of appetite is clearly conserved among mammalian species, and involves, at least in part, interactions with various neuroanatomical substrates within the hypothalamus.

The cannabinoid-induced presynaptic inhibition of glutamatergic synaptic input onto guinea pig arcuate POMC neurons is also consistent with that reported in several other regions of the central nervous system, including the prefrontal cortex [46], hippocampus [47,48], PAG [49] and the dorsal motor nucleus of the vagus [14]. As mentioned above, we also found that CB1 receptor antagonism unmasked a tonic inhibition of glutamate release onto POMC neurons, suggesting that endogenous cannabinoids are a principal neuromodulator influencing synaptic input onto these cells. In the hippocampus [50], cerebellum [51], ventral tegmental area [52] and other hypothalamic nuclei [53], endogenous cannabinoids released from postsynaptic neurons in response to depolarizing stimuli retrogradely inhibit glutamate release from nerve terminals impinging upon them. Indeed, the retrograde inhibition of glutamatergic synaptic input released by endogenous cannabinoids released from parvocellular neurons in the paraventricular nucleus of the hypothalamus is instrumental in mediating the rapid feedbacks of corticosteroids on the stress axis [53]. In transgenic mice whose POMC neurons are labeled with enhanced green fluorescent protein, however, endogenous cannabinoids retrogradely inhibit GABAergic but not glutamatergic synaptic input onto these cells [54]. This suggests that amino acid neurotransmission within POMC neurons is differentially regulated in the two species. Future studies will determine if endogenous cannabinoids synthesized *de novo* in guinea pig POMC neurons serve to tonically inhibit glutamate neurotransmission in a retrograde fashion. Our finding of a CB1 receptor-mediated activation of an inwardly-rectifying K^+ current in POMC neurons is also in agreement with that observed in AtT20 cells transfected with the CB1 receptor [55], and in oocytes co-expressing the CB1 receptor and GIRK1 channel subtype [56,57]. This current cannot be attributed to other voltage-dependent K^+ currents such as the A-type K^+ current [38], and is virtually identical to that elicited by the activation of $GABA_B$ receptors, which have long been known to couple to GIRK in the arcuate nucleus, preoptic area, supraoptic nucleus and many other regions of the central nervous system [58–61].

Along with the ventromedial nucleus of the hypothalamus, the POMC neurons in the arcuate nucleus are the principal anorexigenic component of the hypothalamic feeding circuitry. These neurons release posttranslational byproducts of POMC such as α-melanocyte-stimulating hormone (α-MSH) β-endorphin, as well as CART that is co-expressed in these cells [34,45]. Indeed, β-endorphin and melanocortin (MC)4 receptor knockout mice display extensive hyperphagia [34] and are resistant to disease-induced cachexia [26], respectively. In addition, the anorexigenic effect of the CB1 receptor antagonist rimonabant is eliminated in CART-deficient transgenic mice [62]. POMC neurons are a key target of the satiety hormone leptin, which not only depolarizes and increases the firing rate of these cells, but also decreases hypothalamic levels of endogenous cannabinoids [25,32,33]. Glutamate increases β-endorphin secretion and POMC gene expression, and glutamatergic synaptic input is observed in POMC neurons in the arcuate nucleus and the nucleus of the tractus solitarius of transgenic mice [54,63,64]. While our findings clearly indicate that POMC neurons are a major hypothalamic locus for the hyperphagic actions of cannabinoids, there are in reality a multiplicity of hypothalamic sites and mechanisms involved in the induction of feeding behavior. For example, cannabinoids increase orexigenic NPY release from hypothalamic explants [65]. On the other hand, NPY neurons do not express CB1 receptors, and so the cannabinoid-induced increase in NPY release is due presumably to a decrease in GABA input onto these cells

[31], much like the retrograde inhibition of GABA release onto orexigenic MCH neurons in the lateral hypothalamus [66]. Moreover, cannabinoid interactions with the brain stem, gut, pancreas and adipose tissue also play a role in the regulation of appetite and energy homeostasis [31]. Nevertheless, the presynaptic inhibition of glutamatergic neurotransmission within guinea pig POMC neurons must account, at least in part, for the cannabinoid-induced hyperphagia observed in the present study.

In conclusion, these results reveal that both endogenous and exogenous cannabinoids stimulate feeding behavior via a mechanism that involves, at least in part, a presynaptic inhibition of glutamate neurotransmission in anorexigenic POMC neurons. Our findings convey important insight into how cannabinoids increase appetite through their interactions with the hypothalamic feeding circuitry.

Acknowledgments

The authors thank Shelley Mach and Michelle Gonzales for their technical assistance. This study was supported by PHS Grant DA00521 and an intramural research grant from Western University (06/IRB/003).

References

1. Williams CM, Kirkham TC. Reversal of Δ^9-THC hyperphagia by SR141716 and naloxone but not dexfenfluramine. Pharmacol. Biochem. Behav 2002;71:341–348.
2. Berry EM, Mechoulam R. Tetrahydrocannabinol and endocannabinoids in feeding and appetite. Pharmac Ther 2002;95:185–190.
3. Wachtel SR, Elsohly MA, Ross SA, Ambre J, De Wit H. Comparison of the subjective effects of Δ^9-tetrahydrocannabinol and marijuana in humans. Psychopharmacology (Berl) 2002;161:331–339. [PubMed: 12073159]
4. Cota D, Marsicano G, Lutz B, Vicennati V, Stalla GK, Pasquali R, Pagotto U. Endogenous cannabinoid system as a modulator of food intake. Int J Obesity 2003;27:289–301.
5. Fride E, Bregman T, Kirkham TC. Endocannabinoids and food intake: newborn suckling and appetite regulation in adulthood. Exp Biol Med 2005;230:225–234.
6. Inui A. Cancer anorexia-cachexia syndrome: current issues in research and management. CA Cancer J Clin 2002;52:72–91. [PubMed: 11929007]
7. Woolridge E, Barton S, Samuel J, Osorio J, Dougherty A, Holdcroft A. Cannabis use in HIV for pain and other medical symptoms. J Pain Symptom Manage 2005;29:358–367. [PubMed: 15857739]
8. Hildebrandt AL, Kelly-Sullivan DM, Black SC. Antiobesity effects of chronic CB1 receptor antagonist treatment in diet-induced obese mice. Eur J Pharmacol 2003;462:125–132. [PubMed: 12591104]
9. Cani PD, Montoya ML, Neyrinck AM, Delzenne NM, Lambert DM. Potential modulation of plasma ghrelin and glucagon-like peptide-1 by anorexigenic cannabinoid compounds, SR141716A (rimonabant) and oleoylethanolamide. Br J Nutrition 2004;92:757–761. [PubMed: 15533263]
10. Wierzbicki AS. Rimonabant: endocannabinoid inhibition for the metabolic syndrome. Int J Clin Pract 2006;60:1697–1706. [PubMed: 17109677]
11. Coutts AA, Irving AJ, Mackie K, Pertwee RG, Anavi-Goffer S. Localisation of cannabinoid CB_1 receptor immunoreactivity in the guinea pig and rat myenteric plexus. J. Comp. Neurol 2002;448:410–422.
12. Pertwee RG. Cannabinoids and the gastrointestinal tract. Gut 2001;48:859–867. [PubMed: 11358910]
13. Burdyga G, Lal S, Varro A, Dimaline R, Thompson DG, Dockray GJ. Expression of cannabinoid CB1 receptors by vagal afferent neurons is inhibited by cholecystokinin. J Neurosci 2004;24:2708–2715. [PubMed: 15028763]
14. Derbenev AV, Stuart TC, Smith BN. Cannabinoids suppress synaptic input to neurones of the rat dorsal motor nucleus of the vagus nerve. Physiol 2004;559:923–938.
15. Edwards CMB, Abusnana S, Sunter D, Murphy KG, Ghatei MA, Bloom SR. The effect of the orexins on food intake: comparison with neuropeptide Y, melanin-concentrating hormone and galanin. J Endocrinol 1999;160:R7–R12. [PubMed: 10077743]

16. Ballinger AB, Williams G, Corder R, El-Haj T, Farthing MJG. Role of hypothalamic neuropeptide Y and orexigenic peptides in anorexia associated with experimental colitis in the rat. Clin Sci 2001;100:221–229. [PubMed: 11171292]
17. Della-Zuana O, Presse F, Ortola C, Duhault J, Nahon JL, Levens N. Acute and chronic administration of melanin-concentrating hormone enhances food intake and body weight in Wistar and Sprague-Dawley rats. Int J Obesity 2002;26:1289–1295.
18. Abbott CR, Kennedy AR, Wren AM, Rossi M, Murphy KG, Seal LJ, Todd JF, Ghatei MA, Small CJ, Bloom SR. Identification of hypothalamic nuclei involved in the orexigenic effect of melanin-concentrating hormone. Endocrinology 2003;144:3943–3949. [PubMed: 12933668]
19. Kotz CM, Grace MK, Briggs JE, Billington CJ, Levine AS. Naltrexone induces arcuate nucleus neuropeptide Y gene expression in the rat. Am J Physiol Regul Integr Comp Physiol 1996;271:R289–R294.
20. Glaum SR, Hara M, Bindokas VP, Lee CC, Polonsky KS, Bell GI, Miller RJ. Leptin, the *obese* gene product, rapidly modulates synaptic transmission in the hypothalamus. Mol. Pharmacol 1996;50:230–235.
21. Kalra SP, Horvath TL. Neuroendocrine interactions between galanin, opioids and neuropeptide Y in the control of reproduction and appetite. Ann NY Acad Sci 1998;863:236–240. [PubMed: 9928174]
22. Smith MS, Grove KL. Integration of the regulation of reproductive function and energy balance: lactation as a model. Frontiers Neuroendocrinol 2002;23:225–256.
23. Toshinai K, Date Y, Murakami N, Shimada M, Mondal MS, Shimbara T, Guan JL, Wang QP, Funahashi H, Sakurai T, Shioda S, Matsukura S, Kangawa K, Nakazato M. Ghrelin-induced food intake is mediated via the orexin pathway. Endocrinology 2003;144:1506–1512. [PubMed: 12639935]
24. Varma M, Laviano A, Meguid MM, Gleason JR, Yang ZJ, Oler A. Comparison of early feeding pattern dynamics in female and male rats after reversible ventromedial nucleus of hypothalamus block. J Investig Med 2000;48:417–4262.
25. Cowley MA, Cone RD, Enriori P, Louiselle I, Williams SM, Evans AE. Electrophysiological actions of peripheral hormones on melanocortin neurons. Ann NY Acad Sci 2003;994:175–186. [PubMed: 12851314]
26. Marks DL, Cone RD. The role of the melanocortin-3 receptor in cachexia. Ann NY Acad Sci 2003;994:258–266. [PubMed: 12851324]
27. Cota D, Marsicano G, Tschöp M, Grübler Y, Flachskamm C, Schubert M, Auer D, Yassouridis A, Thöne-Reineke C, Ortmann S, Tomassoni F, Cervino C, Nisoli E, Linthhorst ACE, Pasquali R, Lutz B, Stalla GK, Pagotto U. The endogenous cannabinoid system affects energy balance via central orexigenic drive and peripheral lipogenesis. J Clin Invest 2003;112:423–431. [PubMed: 12897210]
28. Zorilla EP, Taché Y, Koob GF. Nibbling at the CRF receptor control of feeding and gastrointestinal motility. Trends Pharmacol Sci 2003;24:421–427. [PubMed: 12915052]
29. Goldsmith PC, Boggan JE, Thind KK. Opioid synapses on vasopressin neurons in the paraventricular and supraoptic nuclei of juvenile monkeys. Neuroscience 1991;45:709–719. [PubMed: 1775244]
30. Horvath TL. Endocannabinoids and the regulation of body fat: the smoke is clearing. J Clin Invest 2003;113:323–326. [PubMed: 12897199]
31. Matias I, Di Marzo V. Endocannabinoids and the control of energy balance. Trends Endocrinol Metab 2007;18:27–37. [PubMed: 17141520]
32. Di Marzo V, Goparahu SK, Wang L, Liu J, Bátkai S, Járai Z, Fezza F, Miura GI, Palmiter RD, Sugiura T, Kunos G. Leptin-regulated endocannabinoids are involved in maintaining food intake. Nature 2001;410:822–825. [PubMed: 11298451]
33. Plum L, Ma X, Hampel B, Balthasar N, Coppari R, Münzberg H, Shanabrough M, Burdakov D, Rother E, Janoschek R, Alber J, Belgardt BF, Koch L, Seibler J, Schwenk F, Fekete C, Suzuki A, Mak TW, Krone W, Horvath TL, Ashcroft FM, Brüning JC. Enhanced PIP_3 signaling in POMC neurons causes K_{ATP} channel activation and leads to diet-sensitive obesity. J. Clin. Invest 2006;116:1886–1901.
34. Low MJ, Hayward MD, Appleyard SM, Rubinstein M. State-dependent modulation of feeding behavior by proopiomelanocortin-derived β-endorphin. Ann NY Acad Sci 2003;994:192–201. [PubMed: 12851316]

35. Horton BJ, West CE, Turley SD. Diurnal variation in the feeding pattern of guinea pigs. Nutr Metabol 1975;18:294–301.

36. Odumosu A. Vitamin C and weight reducing drugs on brain ascorbic acid in guinea pigs. Acta Vitaminol Enzymol 1981;3:96–102. [PubMed: 7325103]

37. Sherrill RG, Berman JM, Birkemo L, Croom DK, Dezube M, Ervin GN, Grizzle MK, James MK, Johnson MF, Queen KL, Rimele TJ, Vanmiddlesworth F, Sugg EE. 1,4-Benzodiazepine peripheral cholecystokinin (CCK-A) receptor agonists. Bioorg Med Chem Lett 2001;11:1145–1148. [PubMed: 11354363]

38. Tang SL, Tran V, Wagner EJ. Sex differences in the cannabinoid modulation of an Atype K^+ current in neurons of the mammalian hypothalamus. J. Neurophysiol 2005;94:2983–2986.

39. Ronnekleiv OK, Loose MD, Erickson KR, Kelly MJ. A method for immunocytochemical identification of biocytin-labeled neurons following intracellular recording. BioTechniques 1990;9:432–438. [PubMed: 1979496]

40. Weber E, Evans CJ, Chang JK, Barchas JD. Antibodies specific for α-N-acetyl-β-endorphins: Radioimmunoassays and detection of acetylated β-endorphins in pituitary extracts. J Neurochem 1982;38:436–447. [PubMed: 6809901]

41. Cota D, Tschöp MH, Horvath TL, Levine AS. Cannabinoids, opioids and eating behavior: the molecular face of hedonism? Brain Res. Rev 2006;51:85–107.

42. Van Sickle MD, Duncan M, Kingsley PJ, Mouihate A, Urbani P, Mackie K, Stella N, Makriyannis A, Piomelli D, Davison JS, Marnett LJ, Di Marzo V, Pittman QJ, Patel KD, Sharkey KA. Identification and functional characterization of brainstem cannabinoid CB_2 receptors. Science 2005;310:329–332. [PubMed: 16224028]

43. Avraham Y, Menachem AB, Okun A, Zlotarav O, Abel N, Mechoulam R, Berry EM. Effects of the endocannabinoid noladin ether on body weight, food consumption, locomotor activity, and cognitive index in mice. Brain Res Bull 2005;65:117–123. [PubMed: 15763177]

44. Itateyama E, Chiba S, Sakata T, Yoshimatsu H. Hypothalamic neuronal histamine in genetically obese animals: its implication of leptin action in the brain. Exp Biol Med 2003;228:1132–1137.

45. Horvath TL. The hardship of obesity: a soft-wired hypothalamus. nature neuroscience 2005;8:561–565.

46. Auclair N, Otani S, Soubrie P, Crepel F. Cannabinoids modulate synaptic strength and plasticity at glutamatergic synapses of rat prefrontal cortex pyramidal neurons. J Neurophysiol 2000;83:3287–3293. [PubMed: 10848548]

47. Shen MX, Piser TM, Seybold VS, Thayer SA. Cannabinoid receptor agonists inhibit glutamatergic synaptic transmission in rat hippocampal cultures. J Neurosci 1996;16:4322–4334. [PubMed: 8699243]

48. Straiker AJ, Borden CR, Sullivan JM. G-protein α subunit isoforms couple differentially to receptors that mediate presynaptic inhibition at rat hippocampal synapses. J Neurosci 2002;22:2460–2468. [PubMed: 11923410]

49. Vaughan CW, Connor M, Bagley EE, Christie MJ. Actions of cannabinoids on membrane properties and synaptic transmission in rat periaqueductal gray neurons in vitro. Mol Pharmacol 2000;57:288–295. [PubMed: 10648638]

50. Ohno-Shosaku T, Tsubokawa H, Mizushima I, Yoneda N, Zimmer A, Kano M. Presynaptic cannabinoid sensitivity is a major determinant of depolarization-induced retrograde suppression at hippocampal synapses. J Neurosci 2002;22:3864–3872. [PubMed: 12019305]

51. Maejima T, Ohno-Shosaku T, Kano M. Endogenous cannabinoid as a retrograde messenger from depolarized postsynaptic neurons to presynaptic terminals. Neurosci Res 2001;40:205–210. [PubMed: 11448511]

52. Melis M, Perra S, Muntoni AL, Pillolla G, Lutz B, Marsicano G, Di Marzo V, Gessa GL, Pistis M. Prefrontal cortex stimulation induces 2-arachidonoyl-glycerol-mediated suppression of excitation in dopamine neurons. J Neurosci 2004;24:10707–10715. [PubMed: 15564588]

53. Di S, Malcher-Lopes R, Halmos KC, Tasker JG. Nongenomic glucocorticoid inhibition via endocannabinoid release in the hypothalamus: a fast feedback mechanism. J Neurosci 2003;23:4850–4857. [PubMed: 12832507]

54. Hentges ST, Low MJ, Williams JT. Differential regulation of synaptic inputs by constitutively released endocannabinoids and exogenous cannabinoids. J Neurosci 2005;25:9746–9751. [PubMed: 16237178]
55. Mackie K, Lai Y, Westenbroek R, Mitchell R. Cannabinoids activate an inwardly rectifying potassium conductance and inhibit Q-type calcium currents in AtT20 cells transfected with rat brain cannabinoid receptor. J Neurosci 1995;15:6552–6561. [PubMed: 7472417]
56. Henry DJ, Chavkin C. Activation of inwardly rectifying potassium channels (GIRK1) by co-expressed rat brain cannabinoid receptors in *Xenopus* oocytes. Neurosci. Lett 1995;186:91–94.
57. McAllister SD, Griffin G, Satin LS, Abood ME. Cannabinoid receptors can activate and inhibit G protein-coupled inwardly rectifying potassium channels in a *Xenopus* oocyte expression system. J. Pharmacol. Exp. Ther 1999;291:618–626.
58. Wagner EJ, Bosch MA, Kelly MJ, Rønnekleiv OK. A powerful $GABA_B$ receptor-mediated inhibition of GABAergic neurons in the arcuate nucleus. Neuroreport 1999;10:2681–2687. [PubMed: 10574392]
59. Wagner EJ, Rønnekleiv OK, Bosch MA, Kelly MJ. Estrogen biphasically modifies hypothalamic GABAergic neuronal function concomitantly with negative and positive control of luteinizing hormone release. J Neurosci 2001;21:2085–2093. [PubMed: 11245692]
60. Davila V, Yan Z, Craciun LC, Logothetis D, Sulzer D. D_3 dopamine autoreceptors do not activate G-protein-gated inwardly rectifying potassium channel currents in substantia nigra dopamine neurons. J. Neurosci 2003;23:5693–5697.
61. Slugg RM, Zheng SX, Fang Y, Kelly MJ, Rønnekleiv OK. Baclofen inhibits guinea pig magnocellular neurons via activation of an inwardly-rectifying K^+ conductance. J Physiol (Lond) 2003;551:295–308. [PubMed: 12813153]
62. Osei-Hyiaman D, Depetrillo M, Harvey-White J, Bannon AW, Cravatt BF, Kuhar MJ, Mackie K, Palkovits M, Kunos G. Cocaine- and amphetamine-related transcript is involved in the orexigenic effect of endogenous anandamide. Neuroendocrinology 2005;81:273–282. [PubMed: 16131814]
63. Yang ZY, Copolov DL, Lim AT. Glutamate enhances the adenylyl cyclase-cAMP system-induced beta- endorphin secretion and POMC mRNA expression in rat hypothalamic neurons in culture: NMDA receptor-mediated modulation. Brain Res 1995;692:129–136. [PubMed: 8548296]
64. Appleyard SM, Bailey TW, Doyle MW, Jin YH, Smart JL, Low MJ, Andresen MC. Proopiomelanocortin neurons in nucleus tractus solitarius are activated by visceral afferents: regulation by cholecystokinin and opioids. J Neurosci 2005;25:3578–3585. [PubMed: 15814788]
65. Gamber KM, Macarthur H, Westfall TC. Cannabinoids augment the release of neuropeptide Y in the rat hypothalamus. Neuropharmacology 2005;49:646–652. [PubMed: 15949823]
66. Jo YH, Chen YJL, Chua SC, Talmage DA, Role LW. Integration of endocannabinoid and leptin signaling in an appetite-related neural circuit. Neuron 2005;48:1055–1066. [PubMed: 16364907]

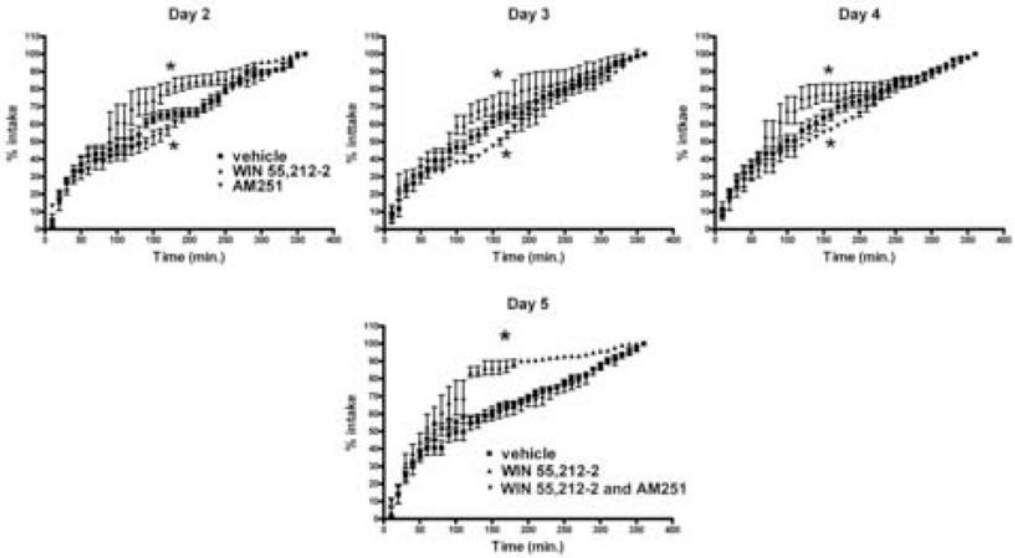

Fig. 1.

The effects of CB1 receptor activation and blockade on the rate of food intake in male guinea pigs observed on representative days over the seven-day monitoring period. Animals were injected daily with either the CB1 receptor agonist WIN 55,212-2 (1 mg/kg; s.c.), the CB1 receptor antagonist AM 251 (3 mg/kg; s.c.), WIN 55,212-2 and AM251 or their cremephor/ethanol/0.9% saline vehicle, introduced into their respective feeding cages and monitored over a six-hour window. For clarity of illustration, days 2–4 show only the effects of WIN 55,212-2 and AM251 *per se*, whereas day 5 shows only the effect of WIN 55,212-2 alone and in combination with AM251. Symbols represent the mean and vertical lines 2 S.E.M. of the cumulative amount of food consumed at 10-minute intervals normalized to the total amount consumed at the end of the six hour window. *, Effects of WIN 55,212-2 and AM251 on the rate of food intake that are significantly different (multi-factorial ANOVA/LSD; $p<0.05$) than those observed either in vehicle-treated controls or in the presence of the other drug.

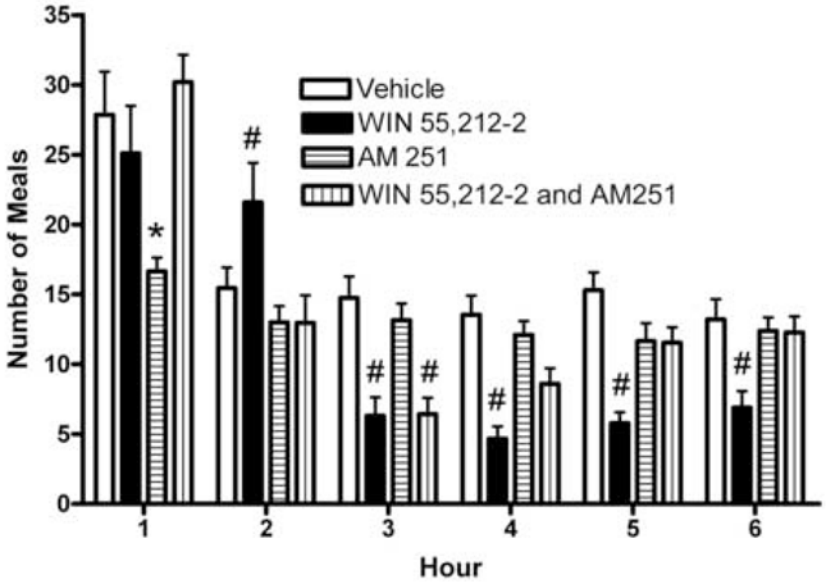

Fig. 2.

The effects of CB1 receptor activation and blockade on meal frequency. The vertical bars represent means and vertical lines 1 S.E.M. of the meal frequency defined as the number of meals eaten per hour over the six-hour monitoring window. #, Values from animals treated with WIN 55,212-2 that are significantly different (ANOVA/median-notched box-and-whisker analysis; $p<0.05$) than those observed in vehicle-treated controls. *, Values from AM251-treated animals that are significantly different (ANOVA/median-notched box-and-whisker analysis; $p<0.05$) than those from vehicle-treated controls.

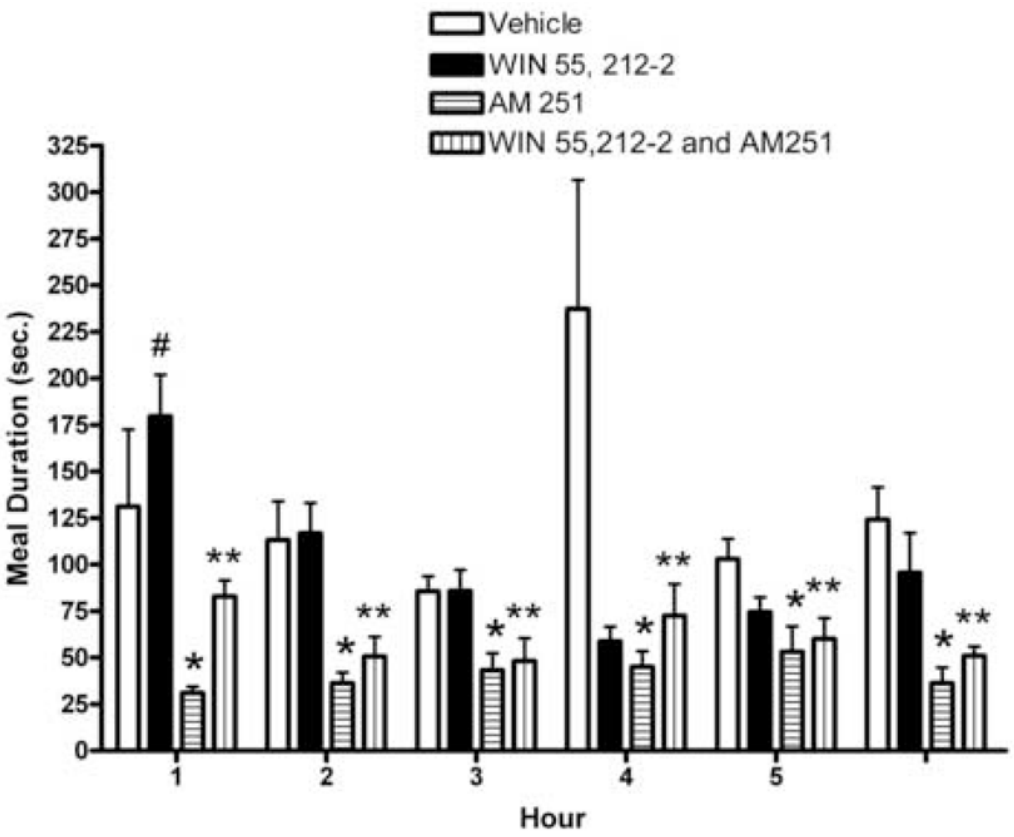

Fig. 3.

The effects of CB1 receptor activation and blockade on meal duration. The vertical bars represent means and vertical lines 1 S.E.M. of the meal duration defined as the time necessary to ingest an amount of food ≥ 10 mg. #, Values from animals treated with WIN 55,212-2 that are significantly different (ANOVA/median-notched box-and-whisker analysis; $p<0.05$) than those from both vehicle-treated animals. *, Values from AM251-treated animals that are significantly different (ANOVA/median-notched box-and-whisker analysis; $p<0.05$) than those from vehicle-treated animals. **, Values from animals treated with both WIN 55,212-2 and AM251 that are significantly different (ANOVA/median-notched box-and-whisker analysis; $p<0.05$) than those observed in animals treated with AM251 alone.

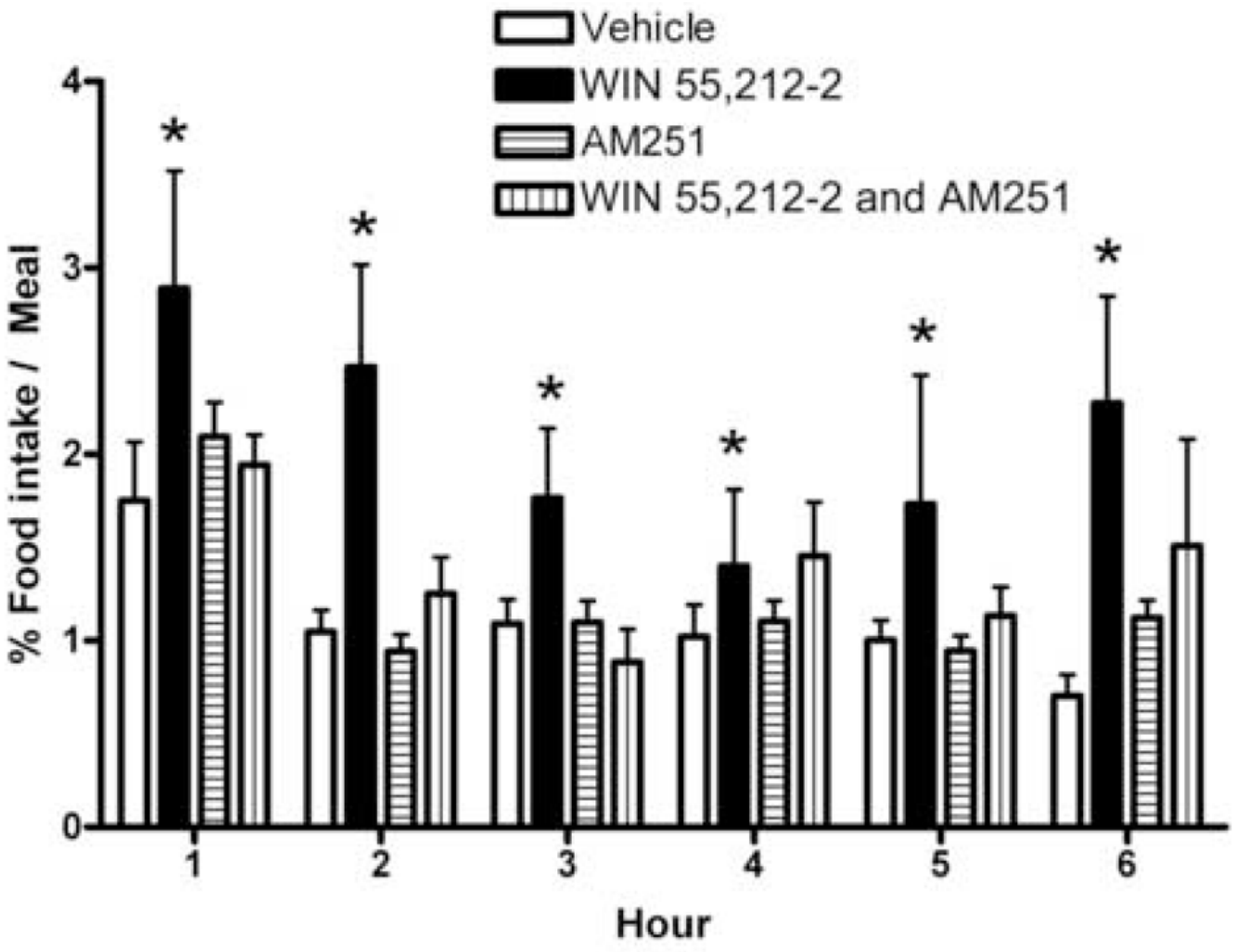

Fig. 4.

The effects of CB1 receptor activation and blockade on the amount of food eaten per meal. Vertical bars signify means and lines 1 S.E.M. of the amount of food consumed in a given hour divided by the number of meals in that same hour. *, Values from animals treated with WIN 55212-2 that are significantly different (ANOVA/LSD; $p<0.05$) than those from vehicle-treated controls.

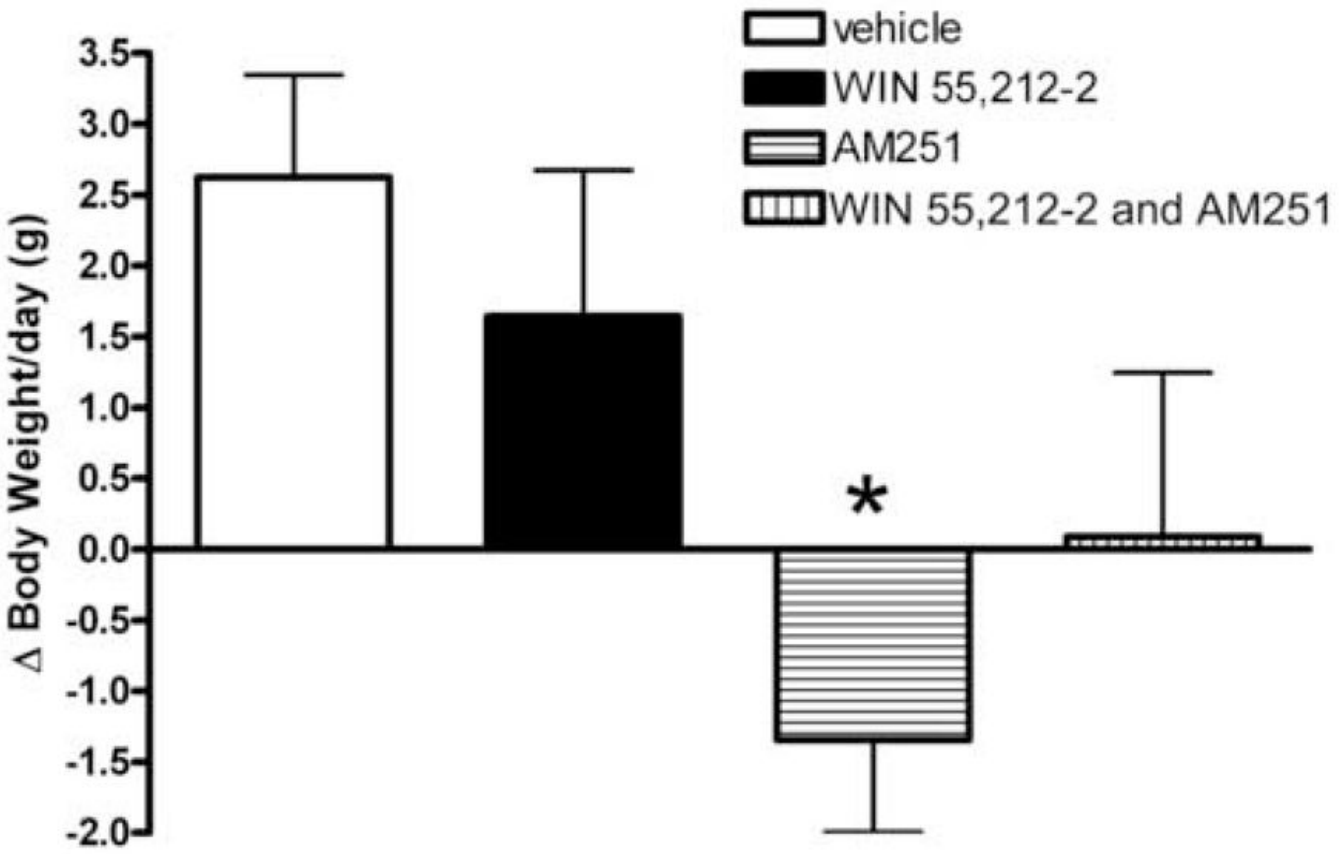

Fig. 5.

The effects of CB1 receptor activation and blockade on the rate of weight change. The vertical bars represent means and vertical lines 1 S.E.M. of the change in body weight per day. *, Values from AM251-treated animals that are significantly different (ANOVA/median-notched box-and-whisker analysis; $p<0.05$) than those from vehicle-treated animals.

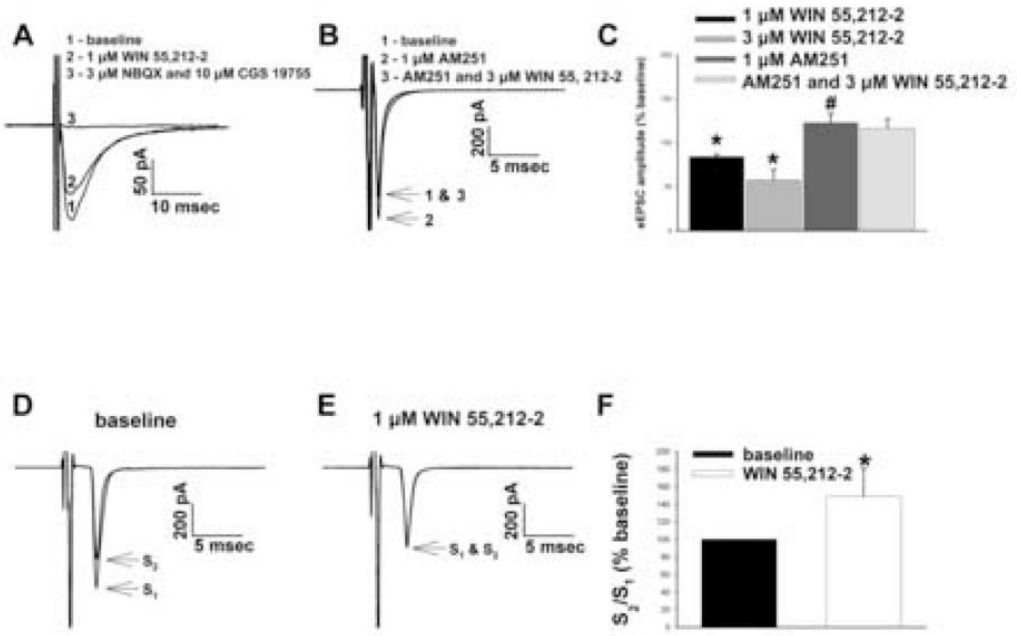

Fig. 6.

A, WIN 55,212-2 attenuates glutamatergic eEPSCs in arcuate neurons. Currents were generated via a concentric bipolar tungsten stimulating electrode at a holding potential of −75 mV in the presence of 10 μM SR 95531. Compared to the eEPSCs elicited under baseline control conditions (1), WIN 55,212-2 reduced peak amplitude (2) of eEPSCs that were completely ablated by NBQX and CGS 19755 (3). **B**, AM251 prevents the cannabinoid-induced decrease in eEPSC amplitude. AM251 *per se* increased eEPSC amplitude (2) relative to baseline control currents (1), and reversed the inhibitory effect of WIN 55,212-2 (3). **C**, Composite bar graph that illustrates the CB1 receptor-mediated reduction in glutamatergic eEPSCs. Columns represent means and vertical lines 1 S.E.M. (n = 6) of the eEPSC amplitudes that were normalized to their respective baseline control values (−435.4 ± 247.6 pA; n = 16). *, Peak eEPSC amplitudes seen in the presence of WIN 55,212-2 that were significantly different (Kruskal-Wallis/Mann-Whitney U-test; $p<0.05$) than those observed under baseline control conditions. #, Values of eEPSC amplitude observed in the presence of AM251 that were significantly different (Kruskal-Wallis/Mann-Whitney U-test; $p<0.05$) than their respective baseline control values. **D & E**, Glutamatergic EPSCs evoked in an arcuate neuron using the paired-pulse paradigm under baseline conditions (**D**), and in the presence of WIN 55,212-2 (**E**). Paired stimuli are separated by 75 msec. **F**, A bar graph that illustrates the agonist-induced increase in the S2:S1 ratio. Vertical bars represent means and vertical lines 1 S.E.M. of the S2:S1 ratios observed under baseline control (solid column) and agonist-treated (open column) conditions that were normalized to control values (0.9 ± 0.2; n = 3).

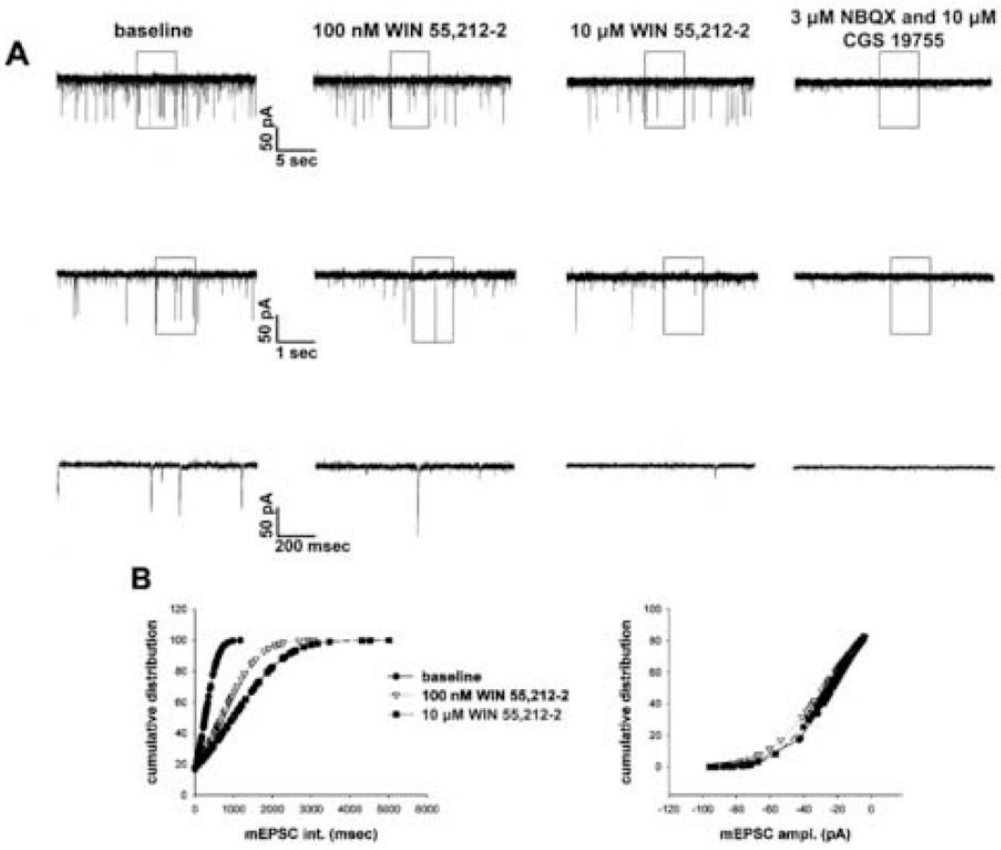

Fig. 7.

WIN 55,212-2 selectively decreases the frequency of glutamatergic mEPSCs in arcuate neurons. **A**, Membrane current traces showing the spontaneous mEPSCs recorded in an arcuate neuron at a holding potential of −75 mV in the presence of 10 μM SR 95531 and 500 nM TTX. The middle traces represent excerpts from expanded portions of their respective upper traces that are contained within the bracket. The lower traces, in turn, represent excerpts from expanded portions of their respective middle traces that are contained within the bracket. The frequency of the robust mEPSCs occurring under baseline control condition (left) is reduced by 100 nM WIN 55,212-2 (middle), and still further by 10 μM WIN 55,212-2 (right). **B,** Cumulative probability plot on the left illustrating the increase in the interval, which is the inverse of frequency, between contiguous mEPSCs observed in the cell in **A**. On the right is a cumulative probability plot showing that WIN 55,212-2 has no discernable effect on mEPSC amplitude.

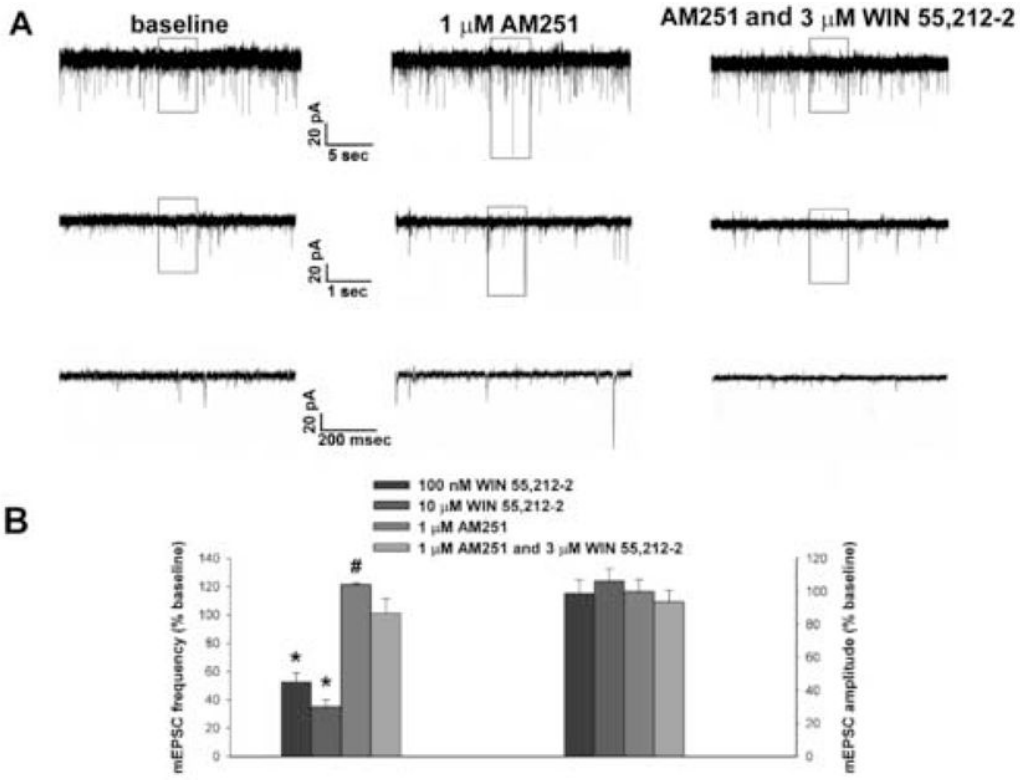

Fig. 8.

AM251 increases glutamatergic mEPSC frequency, and blocks the inhibitory effect of WIN-55,212-2. **A**, Membrane current traces recorded in an arcuate neuron. The middle traces represent expanded portions of their respective upper traces that are contained within the rectangle. The lower traces, in turn, enlarged segments of their respective middle traces that are contained within the rectangle. Note that AM251 alone increases the number mEPSCs, whereas in combination with WIN 55,212-2 the number of mEPSCs is nearly identical to that observed under baseline control conditions. **B**, Composite bar graph demonstrating the selective CB1 receptor-mediated decrease in mEPSC frequency but not amplitude. Columns represent means and vertical lines 1 S.E.M. (n = 3 – 5) of the mEPSC frequency (left) and amplitude (right) values that were normalized to their respective control values (4.0 ± 0.7 Hz; −13.2 ± 2.2 pA; n = 20). *, Values of mEPSC frequency observed in the presence of WIN 55,212-2 that were significantly different (Kruskal-Wallis/Mann-Whitney U-test; $p<0.05$) than those encountered under baseline control conditions. #, Values of mEPSC frequency observed in the presence of AM251 that were significantly different (Kruskal-Wallis/Mann-Whitney U-test; $p<0.05$) than their respective baseline control values.

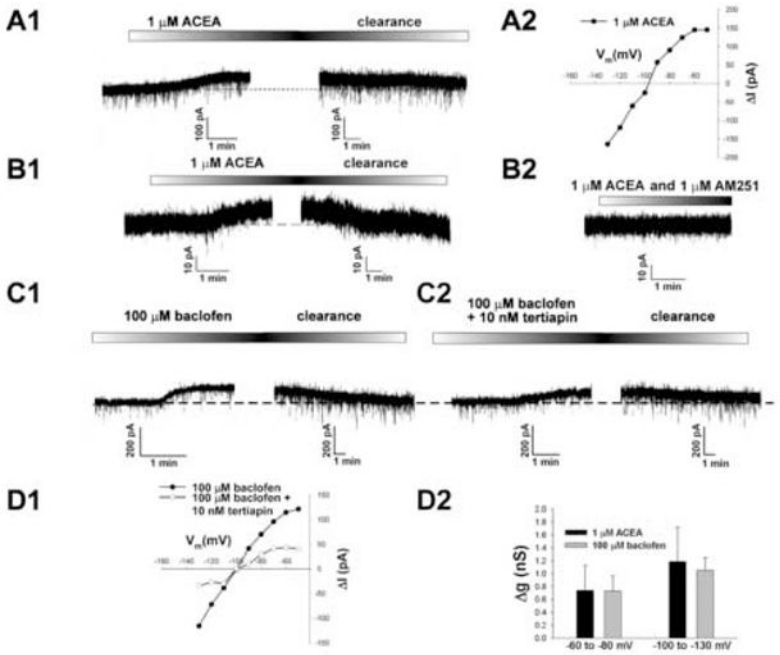

Fig. 9.

A1, A reversible outward current elicited by the anandamide derivative ACEA in an arcuate neuron from an intact male guinea pig. This outward current was produced by ACEA (1 μM) from a holding potential of −60 mV in the presence of 1 μM TTX. The break in the trace in the upper panel represents the time necessary to conduct a second I/V relationship, and the early stages of ACEA clearance from the slice. **A2**, An I/V plot that reveals the ACEA-induced increase in slope conductance as well as the reversal potential (−97 mV) near the Nernst equilibrium potential for K^+. The symbols represent the changes in membrane current (ΔI) observed at different membrane voltages (V_m) that were caused by ACEA. The increase in slope conductance estimated by linear regression between −60 & −80 mV was (2.75 nS), whereas that between −100 & −130 mV was even greater (4.76 nS; rectification ratio: 1.7). **B1**, Another example of the CB1 receptor-mediated outward current recorded in an arcuate neuron from a male guinea pig. As with **A1**, this reversible, ACEA-induced outward current (12.2 pA at −60 mV) was observed in the presence of 1 μM TTX. The break in the trace represents the time necessary to conduct a second I/V in the presence of drug, as well as the early stages of drug clearance from the slice. **B2**, This trace shows the effect of ACEA observed in the presence of the CB1 receptor antagonist AM251 (1 μM). The data was obtained from the same neuron as in **B1**. Note that AM251 completely blocked the ACEA-induced outward current. **C1**, The $GABA_B$ receptor-mediated activation of GIRK in an arcuate neuron from a male guinea pig. This panel shows the reversible, outward current elicited by the $GABA_B$ receptor agonist baclofen (100 μM) from a holding potential of −60 mV in the presence of 1 μM TTX. The break in the trace represents the time necessary to complete a second I/V relationship, and the early stages of drug clearance from the slice. **C2**, The attenuation in the $GABA_B$ receptor-mediated activation of the outward current by the GIRK channel blocker tertiapin in the arcuate neuron shown in **C1**. This panel shows the reduction in the reversible, baclofen-induced outward current in the presence of TTX and tertiapin (10 nM). The break in the trace represents the time necessary to complete a second I/V relationship, and the early stages of drug clearance from the slice. **D1**, This panel shows an I/V plot revealing the baclofen-induced increase in slope conductance and the reversal potential (−100 mV) that closely approximates the Nernst equilibrium potential for K^+. The symbols represent the change in membrane current (ΔI) observed at different membrane voltages (V_m) that were caused by

baclofen (solid circles) or by baclofen in the presence of tertiapin (open circles). The slope conductance estimated by linear regression between −60 & −80 mV was 2.23 nS, and that observed between −100 & −130 mV was even greater (3.78 nS; rectification ratio: 1.7). Tertiapin reduced this baclofen-induced increase in the slope conductance nearly 70% (to 0.7 nS) between −60 & −80 mV, and nearly 75% (to 1.00 nS) between −100 & −130 mV. **D2**, , A bar graph showing the change in slope conductance (Δ g) evoked by CB1 and $GABA_B$ receptor activation at different portions of individual I/V plots. Agonist-induced Δ g is estimated by linear regression between −60 & −80 mV, and between −100 & −130 mV. Columns represent the means and vertical lines 1 S.E.M. of the Δ g caused by 1 μM ACEA (dark columns; n=7) and 100 μM baclofen (gray columns; n=21).

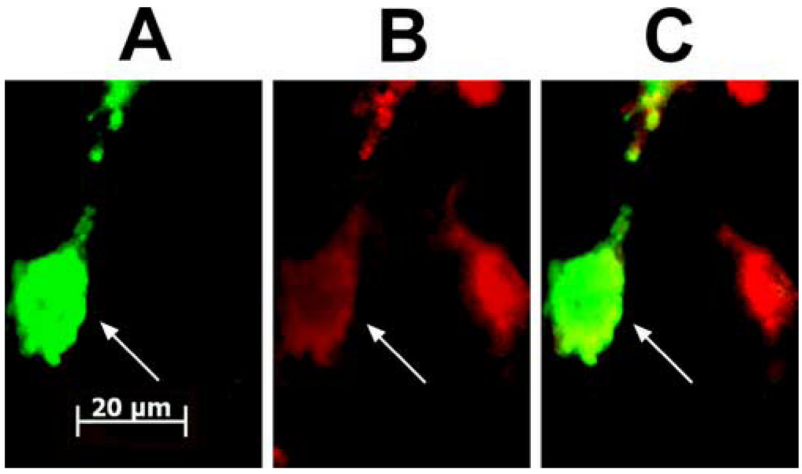

Fig. 10.

Double-labeling of an arcuate neuron that is immunopositive for a phenotypic marker characteristic of POMC neurons. **A**, Color photomicrograph that illustrates the biocytin-streptavidin-cy2 labeling (denoted by the arrow). **B**, Color photomicrograph of the α-MSH immunofluorescence observed in the perikarya of **A** as visualized with cy3 (also denoted by the arrow). **C**, Composite overlay illustrating the double labeling in this arcuate neuron. All photomicrographs were taken with a 40X objective.